Research article

Majid Aalizadeh, Andriy E. Serebryannikov*, Ekmel Ozbay and Guy A. E. Vandenbosch

A simple Mie-resonator based meta-array with diverse deflection scenarios enabling multifunctional operation at near-infrared

https://doi.org/10.1515/nanoph-2020-0386
Received July 8, 2020; accepted August 30, 2020; published online September 29, 2020

Abstract: Deflection, a basic functionality of wavefront manipulation is usually associated with the phase-gradient metasurfaces and the classical blazed gratings. We numerically and experimentally demonstrate an unusually wideband and simultaneously wide-angle deflection achieved at near-infrared in reflection mode for a periodic (nongradient), ultrathin meta-array comprising only one silicon nanorod (Mie resonator) per period. It occurs in the range where only the first negative diffraction order and zero order may propagate. Deflection serves as the enabler for multifunctional operation. Being designed with the main goal to obtain ultra-wideband and wide-angle deflection, the proposed meta-array is also capable in spatial filtering and wide-angle splitting. Spatial filtering of various types can be obtained in one structure by exploiting either deflection in nonzero diffraction orders, or the specular-reflection (zero-order) regime. Thus, the role of different diffraction orders is clarified. Moreover, *on–off* switching of deflection and related functionalities is possible by changing polarization state of the incident wave. The suggested device is simple to fabricate and only requires cost-effective materials, so it is particularly appropriate for the large-area fabrication using nanoprint lithography. Ultra-wideband wide-angle and other deflection scenarios, along with the other functionalities, are promising for applications in optical communications, laser optics, sensing, detection, and imaging.

Keywords: deflection; meta-array; Mie resonance; multifunctionality; spatial filtering; splitting.

1 Introduction

Anomalous refraction and deflection belong to the main scenarios of wavefront manipulation [1–3]. When we tell about deflection, we mean that the outgoing wave deviates from the incident wave direction in transmission mode, after passing through a finite-thickness structure. In reflection mode, we assume that the angle of the outgoing wave differs from that in the case of specular reflection. Two decades ago and even earlier, deflection has been realized in the structures known as blazed gratings, which were designed so that most of the incident wave energy is converted into one of the higher diffraction orders. High-efficiency blazed gratings for wide-angle transmission mode [4], wideband transmission mode [5], and reflection mode [6] have been proposed for operation at the visible and near-infrared frequencies. In particular, designs based on binary gratings and more complex gratings with several ridges per period [4, 6, 7] and artificial dielectrics [5] were used. Multilevel diffraction gratings for both transmission and reflection modes should also be mentioned [8].

At the same time, photonic crystal gratings (PhCGs) have been proposed, which exploit the common effect of Bloch mode dispersion and diffraction that appears due to the periodic interfaces [9]. In transmission mode, PhCGs enable wideband and wide-angle suppression of unwanted zero and higher diffraction orders and redistribution of the incident wave energy in favor of the nonzero order(s) that yield deflection [9–11]. However, high-efficiency deflection which would be simultaneously wideband and wide-angle cannot be obtained in single-wave regime of PhCGs [10]. Single-wave deflection can also be obtained by using an

***Corresponding author: Andriy E. Serebryannikov**, Department of Physics, Adam Mickiewicz University, ul. Uniwersytetu Poznanskiego 2, 61-614 Poznan, Poland, E-mail: andser@amu.edu.pl. https://orcid.org/0000-0001-6896-543X
Majid Aalizadeh, Department of Electrical and Computer Engineering, University of Michigan, Ann Arbor, MI 48109, USA; Nanotechnology Research Center (NANOTAM), Bilkent University, 06800 Ankara, Turkey
Ekmel Ozbay, Nanotechnology Research Center (NANOTAM), Institute of Nanotechnology and Materials Science (UNAM), Department of Physics, Department of Electrical Engineering, Bilkent University, 06800 Ankara, Turkey
Guy A. E. Vandenbosch, ESAT, Katholieke Universiteit Leuven, 3001 Leuven, Flanders, Belgium

epsilon-near-zero (meta)material slab combined with a dielectric grating [12], and a metal grating with sub-wavelength slit(s) or hole(s) that may support surface plasmons [13], but efficiency remains an issue.

In 2011, Yu et al. introduced the generalized refraction law that is connected with the phase discontinuity approach and gradient metasurfaces, which usually have diffraction-free unit cells and enable deflection due to the covering of the whole range of phase variation, i.e., from 0 to 2π [14–16]. Many studies have been dedicated to gradient metasurfaces and meta-arrays based on Pancharatnam–Berry phase (geometric phase), plasmonic resonances, and Mie resonances [2, 17–22]. The basic features of a large part of the gradient metasurfaces like periodic repetition of the 2π-phase range segments (supercells), each containing several or multiple sub-wavelength unit cells, indicate their similarity with the advanced designs of the blazed gratings, e.g., compare [1] with [23, 24]. For example, the transmission-mode blazed grating which was proposed in a study by Ribot et al. [1] enables wideband deflection by using several tens of nanopillars and nanoholes per period (supercell).

While the general trend has been the use of more complex structural compositions within one large period (supercell) for performance enhancement, the opposite trend has recently occurred. Simpler structures, like meta-arrays with just two nanorods per period [3] and gratings with two grooves per period [25] have been utilized to obtain single-wave deflection in the transmission mode. Binary Mie metasurfaces with two-wave deflection [26] and binary meta-holograms [27] should also be mentioned as examples of the functionally capable structures. It is interesting that one nanorod per period can be sufficient to obtain wideband and simultaneously wide-angle deflection in reflection mode, as has been numerically demonstrated for dielectric circular rod [28] and rectangular rod [29] meta-arrays, as well as for all-metal gratings [30]. A high functional capability of such simple structures is not surprising if to keep in mind diverse functionalities that have earlier been demonstrated for periodic arrays of nanorods/microrods of square, rectangular, and circular cross section [31–36]. At microwave frequencies, wideband and wide-angle deflection has recently been demonstrated for reflective gratings having up to three infinitesimally thin strips per period [37].

On the other hand, functionality integration has gained tremendous interest very recently, unlocking the avenue to the next level in device miniaturization and system integration. Demand in multifunctional devices is expected to grow dramatically in the next decade. Various meta-arrays and metasurfaces with capability in wavefront manipulation, including deflection, have been considered from the multifunctionality perspective [38–40]. The possibility of separation of different (groups of) processes either in the space domain [10] or in the frequency domain [41, 42] is often considered as the general condition of multifunctionality, at least when no tunable component is utilized. Various multifunctional scenarios have been demonstrated, which include those with different types of functionalities or different regimes of the same functionality in the neighboring frequency ranges [41–45], at different polarization states [46–49] or different incidence angles [50, 51] at fixed frequency. Merging two functions in one has attracted attention [11, 52–54]. Noticeably, the geometric-phase metasurfaces are intrinsically multifunctional, since they may merge deflection and polarization manipulation in one step, e.g., see [48, 55, 56]. The tunable and reconfigurable metasurfaces may enable even more diversity in terms of functionality [57–60]. Nevertheless, the capability of the structures which do not comprise tunable components in multifunctional operation is also very high.

In this paper, we numerically and experimentally study a periodic meta-array based on Si nanorods working as Mie resonators, which yields an unusually wideband and wide-angle deflection at near-infrared. While high-efficiency single-wave deflection with either wideband or wide-angle features has been earlier investigated in many works, there are just few papers where ultra-wideband wide-angle deflection is theoretically studied, e.g., see [28–30]. We will demonstrate, also by the experiment, that these features can be simultaneously obtained in a simple reflective meta-array enabling multifunctional operation. It will be shown numerically that the large region of strong deflection nearly coincides with the one, in which the first negative diffraction order is the only nonzero order which may propagate. Similarly to some of the theoretical performances proposed in our earlier works [28, 29], only one nanorod per period is required. The designed structure comprises the Si nanorods placed periodically on the top of a SiO_2 buffer layer that is backed with an Ag reflector. In the considered wavelength range which extends from 550 to 2100 nm, the total thickness of the array and the spacer layer is between 0.15λ and $0.6\ \lambda$ (λ is free-space wavelength), i.e., it is comparable with thicknesses of the recently proposed gradient metasurfaces.

The designed deflecting meta-array will be examined for the capability in multifunctional operation. We will show that the obtained deflection serves as enabler of the secondary functionalities, like spatial filtering and splitting, and no additional parameter adjustment is needed for that. It will be demonstrated that single-wave deflection is connected with spatial filtering, which represents the incidence-angle domain analog of spectral filtering [61],

while two-wave deflection can be connected with the wide-angle splitting functionality [28]. The role of the cutoffs of the first negative and the higher diffraction orders in the studied functionalities will be clarified. Two-beam splitting and various types of spatial filtering, which are yielded by deflection in the different diffraction orders, will be investigated numerically. Finally, the effect of polarization state of the incident wave on the possible *on–off* switching of the abovementioned functionalities will be discussed. All these features together with the ease of fabrication indicate that the proposed device is particularly interesting for the practical scenarios of wavefront manipulation.

2 Results and discussion

2.1 Design and fabrication

The reflective meta-array comprising dielectric nanorods of rectangular cross section has been designed with the main goal to obtain ultra-wideband and simultaneously wide-angle wave deflection for the diffraction order $m = -1$ in case of transverse-electric (TE) polarization, i.e., when the electric field vector of the incident wave is parallel to the axes of the nanorods. The basic feature of the proposed multifunctional design is a high permittivity of the rod material, ε_r, that enables low-order Mie resonances at the considered frequency range, similarly to the earlier studied Mie resonances in nanorods of circular cross section [62]. In our design, the array's period is about eight times larger than the side size of each nanorod. No special parameter adjustment is needed, so that there is a wide range of tolerance for structural parameters. The resulting mechanism of directional selectivity differs from the one in [8], in which Bloch modes play a key role. As entry point for design, we have considered the earlier suggested theoretical performances of meta-arrays of circular cross section dielectric rods [28] and arrays of rectangular cross section rods made of a tunable material [29], in which the resulting mechanism also exploits the specific resonant properties of the dielectric rods. It is however distinguished from the mechanism reported for metal gratings [30] because surface plasmons are not expected to be a critical contributor to the resulting functionality of our meta-array and the back-side reflector is the only component of it, which is made of a metal. Details of simulations are given in Supplementary material.

A perspective view of the designed structure and its cross section are schematically shown in Figure 1(a) and (b), respectively. A scanning electron microscopy (SEM) image of the fabricated sample (top view) is presented in Figure 1(c). The structure contains a periodic array of Si nanorods having rectangular cross section, which are patterned on the top of a SiO_2 buffer layer deposited on an Al layer. As shown in Figure 1(b), p, w, h, d, and b denote the period, width of each nanorod, height of each nanorod, thickness of the SiO_2 layer, and thickness of the bottom Al layer, respectively. Thickness of the Al layer, b, is chosen to completely block the transmission. In our design, $b = 150$ nm. The optimized values of p, w, h, and d are equal to 1250, 150, 180, and 150 nm, respectively. The performed simulations confirm that the meta-array has a good fabrication tolerance, i.e., it is quite robust to small deviations of the dimensions from the chosen values. Moreover, even though rather large deviations can moderately affect the resulting performance, the main features such as high efficiency and ultra-wideband behavior may also be preserved. These features do not result from an accidental parameter choice or careful optimization and come rather from the intrinsic nature of this design.

Standard nanofabrication techniques were used. A commercial Silicon wafer was diced into 1 cm^2 pieces. Then, a 1 cm^2 piece of Si wafer was used as the substrate. It has been cleaned by using acetone, isopropanol, and deionized water. The sample was heated up to 40 °C and sonicated while being immersed in each of the aforementioned liquids. After cleaning, a 150 nm thick Al layer was coated over it with the rate of 0.5 Å/s by using a VAKSIS thermal evaporator device at the chamber pressure of 3e-6 to 5e-6 Torr. Next, a 150-nm thick silica layer was coated over the Al layer using VAKSIS electron beam evaporator in the same rate and chamber pressure. Afterward, PMMA was spun over the sample, and an area of 1 mm^2 from the sample surface was patterned, exposed, and developed using electron beam lithography. After that, a 180-nm Si layer was coated over the sample by utilizing the mentioned e-beam evaporator machine. Finally, the sample was patterned to form Si nanorods by applying the lift-off process.

2.2 Ultra-wideband and simultaneously wide-angle deflection

In line with the numerical results, transmittance and absorbance in the designed structure are significantly smaller than reflectance. Thus, although the computations do not neglect absorption and measurement neither, the mth order diffraction efficiency in reflection, r_m, is determined here as the ratio of the power converted to the mth order to the total reflected power, for the sake of convenience. According to the grating equation, the angles of the outgoing waves attributed to diffraction orders, ϕ_m, are given by [63]

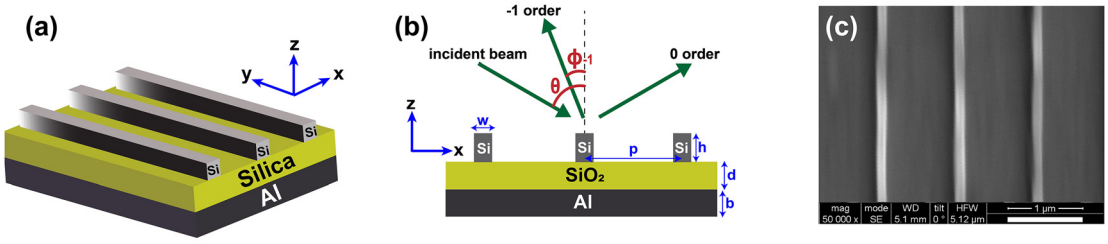

Figure 1: (a) 3D schematic of the structure, (b) 2D cross section of the structure along with the directions of the incident, 0th order reflected, and –1st order diffracted (deflected) beams, and (c) scanning electron microscopy (SEM) image of the fabricated sample (top view). We look for the geometries that funnel the energy into the –1st order, with minimum absorption in the metal and minimum efficiency in the 0th order.

$$\sin\phi_m = \sin\theta + m\lambda/p, \tag{1}$$

with θ being the incidence angle, λ the wavelength, p the period, and $m = 0, \pm1, \pm2, \ldots$. The order $m = 0$ corresponds to specular reflection and propagates at any λ. The orders with $|m| > 0$ may propagate and, thus, contribute to the reflected power only in a finite range of λ variation at $|\sin\phi_m| < 1$. They correspond to the deflected waves.

The capability of our meta-array in deflection at TE polarization is demonstrated in Figure 2. To justify the principal possibility of the wideband deflection, Figure 2(a) presents r_{-1} versus λ for the selected values of θ. A pass band being over 1000 nm wide can be achieved, while the both smaller-λ and larger-λ boundaries of the band are quite sharp. Thus, the meta-array shows a good performance as a spectral filter working in the –1st order. Since $\max r_{-1} > 0.8$ for the all values of θ, the desirably wideband and wide-angle deflection may be expected. To check this guess, we plotted r_{-1} versus θ for the selected values of λ, see Figure 2(b). One can see that the θ-domain pass band is really wide and has quite sharp boundaries, whereas $r_{-1} > 0.85$ and even $\max_{r_{-1}} \approx 1$. Therefore, it is reasonable to study behavior of r_{-1} and r_0 by using the (λ, θ)-plane. In Figure 2(c) and (d), the contour plots of r_m are shown for $m = -1$ and $m = 0$, respectively. It is observed in Figure 2(c) that the structure retains high deflection efficiency for the order $m = -1$ within an ultra-wide λ-range and a wide range of θ variation, so that the incident wave power is dominantly funneled into the –1st order. The remaining energy goes to 0th order and other higher orders in reflection and to absorption (a very small part – also to transmission). It is evident that r_0 (specular reflection) is very low in the region, where r_{-1} is high, compare Figure 2(c) and (d). The contour plots for the orders $m = -4$, -3, -2, and $+1$ are presented in Figures S1 and S2 in Supplementary material.

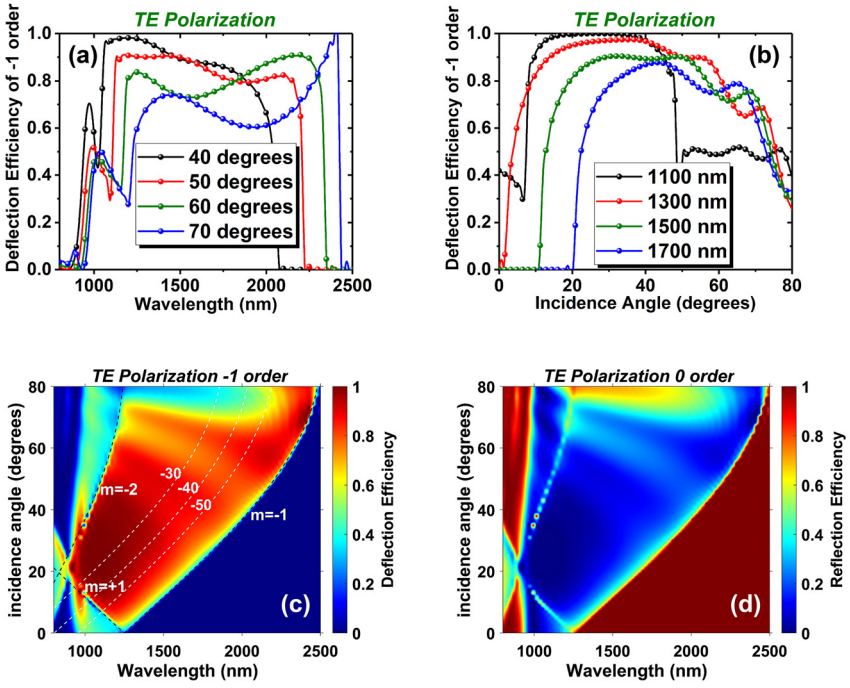

Figure 2: Ultra-wideband and wide-angle deflection in case of TE polarization. Simulated –1st order deflection efficiency, r_{-1}, as a function of (a) wavelength, λ and (b) incidence angle, θ. Contour plots of the simulated deflection/specular reflection efficiency, r_m, for (c) $m = -1$ and (d) $m = 0$. In plot (c), the dashed white lines represent isolines for deflection angle, ϕ_{-1} ($m = -1$), which is equal to –30°, –40°, and –50°; the dashed black lines approximately show cutoffs, i.e., the boundaries of the regions, where the orders $m = -1$, $m = -2$, and $m = +1$ may propagate (on the left side with respect to each of these lines).

The obtained region of the –1st order deflection is unusually large and coincides quite well with the region, in which only this diffraction order is propagating, in addition to 0th order. The ultimate redistribution of the incident wave energy between the propagating diffraction orders occurs at the –1st, –2nd, and +1st order cutoffs, enabling desirably sharp boundaries of the deflection region. The dashed black lines in Figure 2(c) show the cutoffs calculated using Eq. (1). According to Figure 2(c) and (d), at the larger-λ (right) segment of the boundary of the considered deflection range ($1250 < \lambda < 2450$ nm), there is a sharp switching between deflection (r_{-1}) and specular reflection (r_0). The power of the order $m = 0$ immediately drops while entering the –1st order propagation region from the side of larger λ. As seen in Figure 2(c), spectral location and width of the band in the λ-domain depend on θ. The bandwidth increases with θ, and efficiency remains high for a larger part of the band. At $\theta > 50°$, efficiency tends to decrease, so that the choice of θ should be based on the trade-off between bandwidth and efficiency. In turn, bandwidth in the θ-domain depends on λ. In Figure 2(d), it is observed that the regions of the dominant contribution of r_0 are not restricted to the one on the right side from the –1st order cutoff, where all the orders with $|m| > 0$ are evanescent. The case is distinguishable when the 0th order dominates in the region, where the orders with $|m| > 0$ may propagate. This gives us an additional degree of freedom to control the functionality yielded by deflection.

While a detailed study of the possible connection of the studied far-field characteristics and resonances in nanorods is beyond the scope, some features are worth to be mentioned here in the context of resonance type identification. Figure 3 presents the contour maps of the electric field and the quiver maps of the magnetic field in the region inside and around a dielectric nanorod at the selected λ-values. In the quiver maps, the magnitude of the magnetic field at each point is proportional to the length of the arrows. The field distributions in Figure 3(a) and (d) are similar to that of zero-order (azimuthally uniform) resonance of a circular rod/nanocylinder [64]. It can be called as the symmetric zero-order resonance, for the sake of definiteness. The resonance in Figure 3(b) and (e) represents, in fact, a similar but asymmetric resonance (see Figure 4 in [45] for comparison). Finally, the maps in Figure 3(c) and (f) present nothing else than the case of predominant magnetic dipole resonance behavior being similar to that often observed in nanocylinders of small/moderate height, which have been widely used in the recent metasurface studies [17–19]. Broadband resonances with asymmetric field features, like the ones in Figure 3(b) and (e), may be necessary to obtain high-efficiency, wideband, single-wave deflection. The role and the ways of obtaining of such resonances will be a subject of our forthcoming investigations.

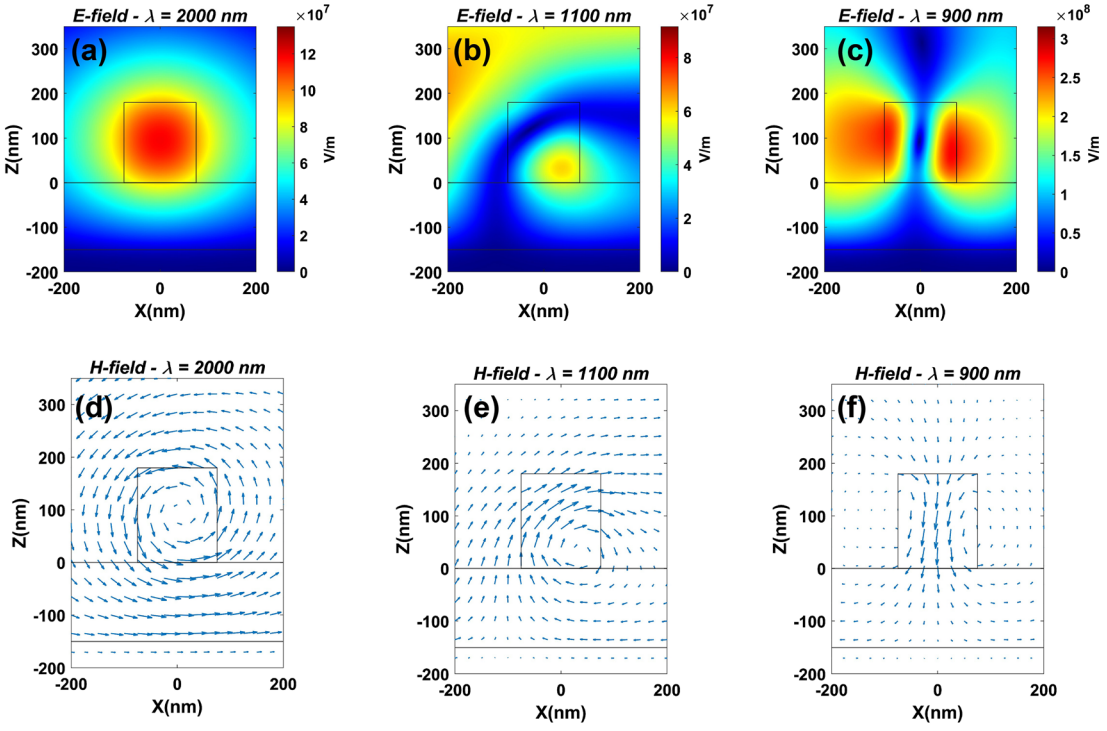

Figure 3: Contour maps of electric field (a–c) and quiver maps of magnetic field (d–f) inside and near a nanorod at (a, d) $\lambda = 2000$ nm, (b, e) $\lambda = 1100$ nm, and (c, f) $\lambda = 900$ nm; $\theta = 20°$, TE polarization.

Examples of the contour maps of electric and magnetic field distribution within a larger region are presented in Figure S3 in Supplementary material.

The capability of the proposed structure to deflect electromagnetic waves in a wide range of θ variation means also that a wide range of the angles of the outgoing wave can be achieved, according to Eq. (1) (see also the isolines of outgoing wave angle in Figure 2(c)). For each of them, the Littrow configuration (back-reflection) regime ($\theta = -\phi_{-1}$, $2\sin\theta = \lambda/p$) is achieved at a particular frequency. At the same time, there is a large region in the (λ, θ)-plane, within which the difference between the directions of the incident and outgoing waves is significant, while high efficiency is kept. For instance, $\phi_{-1} = -50°$ can be obtained when $\theta < 25°$, and $\phi_{-1} = -30°$ when $\theta > 55°$. The outgoing wave angle, θ_{out}, is plotted versus θ and λ in Figure S4 in Supplementary material.

2.3 Experiment

The feasibility study was the aim of the performed experiments, while complete characterization of the suggested design was not. Measurements were carried out by using the J. A. Woollam Co. Inc. VASE Ellipsometer. Two lenses were added and adjusted delicately, one in the source side and the other in the detector side for aligning the incident beam on the patterned area over the sample, and collecting the outgoing-wave radiation through the other lens in the detector side. The measurement range extends from around $\lambda = 1000$ nm up to $\lambda = 1540$ nm. The angle between the incident wave source and detector should be at least 30° that imposes significant restrictions on the used range of θ. The detector arm has the possibility of sweeping the detection angle with a desired step size. First, the base measurements of reflection were carried out by using perfectly reflective mirrors. Then, the measured reflections from the sample were normalized to the base reflection intensity values.

Figure 4 presents the experiment results for the fabricated sample, the SEM image of which is shown in Figure 1(c), and their comparison to the simulations. The contour plots show r_{-1} as a function of λ and θ. Good agreement is achieved, so there is evidence of that the fabricated device enables ultra-wideband, wide-angle, and high-efficiency deflection, as predicted by the numerical results in Figure 2. Some discrepancy between Figure 4(a) and (b) is observed, whose possible causes may include the difference in material parameters, and specifics of illumination and measurements in different ranges of θ, which cannot be entirely taken into account in simulations. Besides, the –2nd order deflection has not been measured and taken into account in normalization applied to the data in Figure 4(a). The experiment ranges of variation in λ and θ are extended from 1000 to 1540 nm, and from 55° to 75°, respectively. These particular ranges were chosen because the detector had to be placed at a specific position for each pair of the values of λ and θ, to measure efficiency of a specific diffraction order of the reflected beam, while the measuring device has restrictions in terms of the position of detector with respect to the source. This is one of the reasons of our focus put in the experimental study on the lower-λ (left) boundary of the –1st order deflection region, which corresponds to the –2nd order cutoff. The second reason is that we would like to experimentally demonstrate a possible sharpness of that particular boundary. That is why the structural parameters were chosen at the design stage to enable its observation in the experiment. Indeed, the ultimate redistribution of the incident wave energy between the orders $m = 0$ and $m = -2$, and the order $m = -1$ at the –2nd order cutoff is less trivial and, thus, more interesting than the energy redistribution between the 0th and –1st orders at the –1st order cutoff, i.e., at the higher-λ (right) boundary. The experiment results confirm that a quite sharp boundary of the –1st order deflection region can be obtained at the –2nd order cutoff. They also show that the θ-domain band width depends on λ that indicates

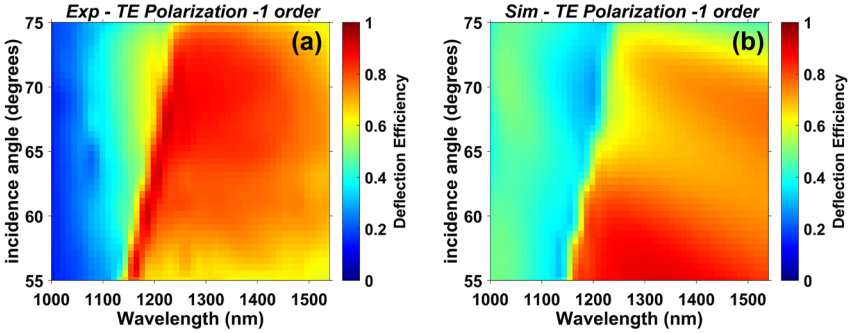

Figure 4: Contour plots presenting (a) experiment and (b) simulation results for –1st order deflection efficiency, r_{-1}, as a function of λ and θ, case of TE polarization. Results are shown within the (λ, θ)-region which is available for the utilized setup.

the principal possibility of multifrequency scenarios and, thus, some scenarios of multifunctional operation.

2.4 Functionalities enabled by deflection

Next, let us revisit the results in Figures 2 and 4 from the point of view of multifunctional operation enabled by ultra-wideband and wide-angle deflection. Spatial filtering is one of the considered functionalities. It is known as the ability of a structure to manifest angular selectivity in transmission or reflection mode (or both), which uses either zero or higher orders. It may result in modifications of the angular spectrum and sorting incident waves. Various performances of spatial filters are known, which are based on interference patterns [65], anisotropic (indefinite) [66], hyperbolic [67] and epsilon-near-zero [68] media, resonant gratings [29, 69, 70], and photonic crystals [28, 61, 71–73].

To obtain spatial filtering in the designed resonant meta-array, we do not need any structural modification of the meta-array as compared to the design enabling wide-angle deflection, since deflection and spatial filtering are, in fact, two sides of the same physical scenario based on the use of nonzero diffraction order(s). Indeed, the sharp boundaries of the high-efficiency single-wave deflection region in the (λ, θ)-plane (region with large r_{-1}), like those observed in the simulation results in Figure 2(b) and (c), and confirmed by the experiment results in Figure 4, indicate the possibility of spatial filtering. The ultra-wideband and simultaneously wide-angle –1st order deflection enabling wideband spatial filtering is probably the most interesting feature of the results discussed in Figures 2(c) and 4. At the same time, the specular-reflection originated (0th order) low-pass spatial filtering regime is possible, see Figure 2(d).

Two specific ranges of λ-variation are observed in Figure 2(c). In the first range, which corresponds to $\pi < kp < 2\pi$ ($1250 < \lambda < 2500$ nm), the order $m = -1$ may propagate within a limited θ-range, according to Eq. (1). Here, –1st order band-pass filtering with a grazing-angle upper-θ boundary and a sharper lower-θ boundary co-exists with the 0th order low-pass filtering. Width and location of the passbands in the θ-domain depend on λ, while location of the lower-θ boundary (θ_{lb}) is determined for the band-pass filtering by Eq. (1) with $m = -1$ and $\sin\phi_{-1} = -1$, i.e.,

$$\theta_{\mathrm{lb}} = \arcsin(\lambda/p - 1). \tag{2}$$

In the second range, which corresponds to $2\pi < kp < 3\pi$ ($833 < \lambda < 1250$ nm), the order $m = -1$ may propagate in the whole θ-range. Here, the both lower and upper boundaries of the –1st order pass band in θ-domain are quite sharp. They appear when an ultimate redistribution of the incident wave energy in favor of the other propagating orders than $m = -1$ takes place. Similarly to the lower-θ boundary of the first range, the upper-θ and lower-θ boundaries of the second range are set by Eq. (1), but now with $m = -2$ and $\sin\phi_{-2} = -1$ and with $m = +1$ and $\sin\phi_{+1} = 1$, respectively, so that

$$\theta_{\mathrm{ub}} = \arcsin(2\lambda/p - 1) \tag{3}$$

and

$$\theta_{\mathrm{lb}} = \arcsin(1 - \lambda/p). \tag{4}$$

Then, the θ-domain band width is given by $\Delta\theta = \theta_{\mathrm{ub}} - \theta_{\mathrm{lb}}$ for the large region of the –1st order deflection. The boundary given by Eq. (3) has been confirmed by the experiment, see Figure 4.

While the (λ, θ)-plane is an efficient tool to summarize the properties of the designed meta-array, the slices of the contour plots for fixed λ can be used to highlight some of the remarkable regimes of spatial filtering. Examples presented in Figure 5(a) and (b) show that a well pronounced narrow band-pass spatial filtering is possible in deflection mode, respectively, at $m = -2$ around $\lambda = 780$ nm for TE polarization, and at $m = -3$ around $\lambda = 550$ nm for transverse-magnetic (TM) polarization, i.e., when the magnetic field vector of the incident wave is parallel to the axes of the nanorods. The bandwidth not exceeding 20° is observed in both Figure 5(a) and (b). Note that in Figure 5(b) it is obtained in the visible range and corresponds to the transition from green to yellow color. The spatial filters in Figure 5(a) and (b) work in a (nearly) back-reflection regime ($\phi_{-2} \approx -\theta$ and $\phi_{-3} \approx -\theta$, respectively). For instance, in Figure 5(b), $\phi_{-3} = -43.5°$ at $\theta = 41°$ and $\lambda = 560$ nm. So far, it is numerically shown that the studied meta-array, in addition to ultra-wideband and wide-angle beam deflection, may yield narrowband deflection in higher diffraction orders and related narrow band-pass spatial filtering. Moreover, bandstop and low-pass spatial filtering can be obtained in the specular-reflection regime ($m = 0$), in the vicinity of 900 nm and between 1500 and 2100 nm, respectively, see Figure 2(d). The spatial filtering regimes that are achieved in the order $m = 0$ are demonstrated in Figure S5 in Supplementary material. To the best of our knowledge, such diversity of spatial filtering regimes in one structure has not been earlier reported.

Now, let us discuss one more functionality enabled in the designed structure by deflection – a wide-angle beam-splitting regime, like the one numerically demonstrated in

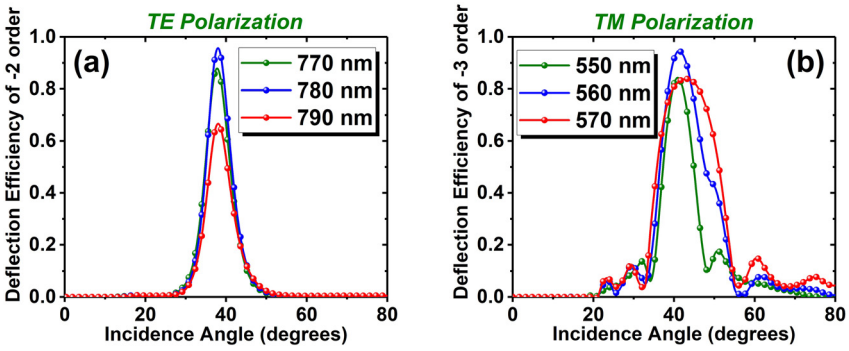

Figure 5: Narrow band pass spatial filtering achievable in the designed meta-array. Simulation results: (a) r_{-2} for TE polarization at the wavelengths of 770,780, and 790 nm, and (b) r_{-3} for TM polarization at the wavelengths of 550, 560, and 570 nm.

[28]. It occurs due to deflection of the orders $m = -1$ and $m = -2$ in a wide range of θ variation that extends over 40°, for TE polarization. It is worth noting that it is uncommon to use the diffraction orders with different $|m|$ for the purposes of splitting. Figure 6(a) and (b) present, respectively, r_{-1} and r_{-2}, as a function of θ, at the selected values of λ. For $\theta > 40°$, we obtain beam splitting between the orders $m = -1$ and $m = -2$ around $\lambda = 1140$ nm. As seen in Figure 6(a) and (b), r_{-1} and r_{-2} are nearly equal when $\theta > 50°$. Thus, the reflected power is almost equally split between the two deflected beams in a very wide θ-range. The −1st order outgoing beam propagates in a nearly normal direction (e.g., $-4.4° < \phi_{-1} < 4°$ at $55° < \theta < 75°$ when $\lambda = 1120$ nm), while the −2nd order outgoing beam's direction significantly differs from both specular reflection and normal direction cases (for example, $-76.6° < \phi_{-2} < -55.7°$ at $55° < \theta < 75°$ when $\lambda = 1120$ nm). Here, the −2nd order beam can be in the back-reflection regime. The simulation and experiment results are compared in Figure 6(c) for $m = -1$. The coincidence is good that confirms the possibility of wide-angle splitting. It should be noted that the discussed splitting regime is not wideband, so that the values of λ should be accurately adjusted. It differs from the ones in polarization beam splitters based on the classical gratings [74] and the recently proposed metasurfaces [54, 75, 76]. The designed meta-array is simpler to fabricate than the known beam splitters using one polarization state [11, 26].

Deflection, spatial filtering, and splitting can be considered as the elementary functionalities, of which multifunctional operation scenarios can be designed. Combinations of the elementary functionalities can be rather arbitrary, depending on the specific requirements connected with particular applications. Clearly, the designed structure may be used in a practical device only

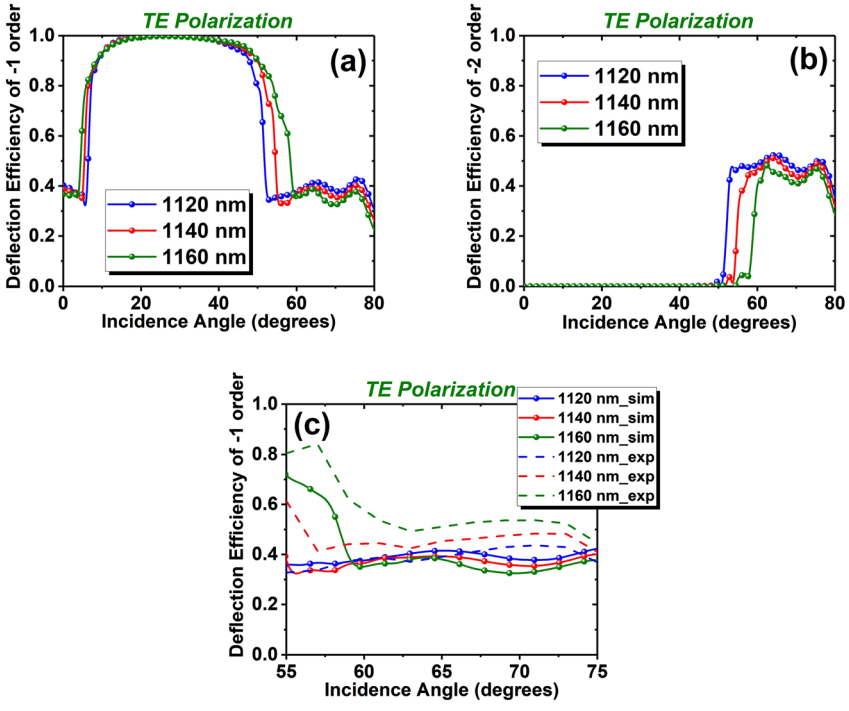

Figure 6: Beam splitter functionality of the designed meta-array.
Simulation results for (a) $m = -1$ and (b) $m = -2$, and (c) comparison of simulation and experiment results for $m = -1$, at the wavelengths of 1120, 1140, and 1160 nm, in case of TE polarization.

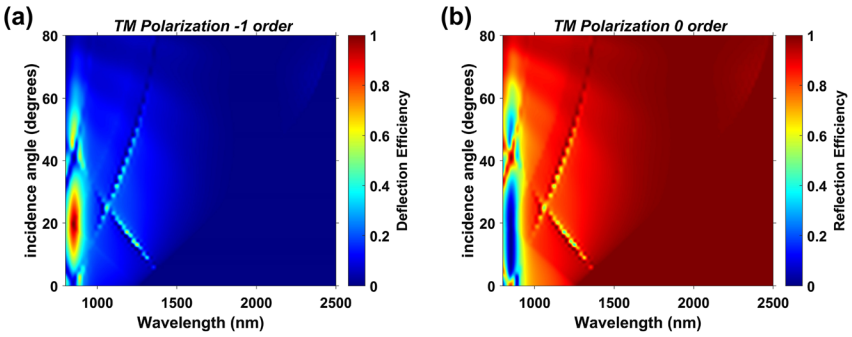

Figure 7: Contour plots of the simulated r_m for (a) $m = -1$ and (b) $m = 0$, case of TM polarization.

for one of the elementary functionalities at a selected wavelength, or within a given wavelength range. Examples of the practical multifunctional operation scenarios may include but are not restricted to (i) θ-dependent deflection at given λ for multiple values of $\theta = \theta_1, \theta_2, \ldots, \theta_m$; (ii) wide band-pass and narrow band-pass spatial filtering, respectively, at $\lambda = \lambda_1$ and $\lambda = \lambda_2$; (iii) wide band-pass spatial filtering with different angular bandwidths at $\lambda = \lambda_1, \lambda_2, \ldots, \lambda_m$; (iv) deflection at $\lambda = \lambda_1$ and splitting at $\lambda = \lambda_2$; (v) wide band-pass or narrow band-pass spatial filtering at $\lambda = \lambda_1$ and splitting at $\lambda = \lambda_2$. Additional functionalities can be obtained by using an incident wave with the wave vector component parallel to the nanorod axes. They will be addressed in a future study.

Finally, the use of both TE and TM polarizations of the incident wave yields one more degree of freedom, enabling polarization sensitive *on–off* switching scenarios. The results for TM polarization are presented in Figure 7, being the counterpart of the results for TE polarization in Figure 2(c) and (d). It is observed that r_{-1} is generally weak for TM polarization in the same large region on the (λ, θ)-plane where the order $m = -1$ dominates for TE polarization, compare Figures 2(c) and 7(a). For further clarity, Figure S6 in Supplementary material presents r_0 versus θ in case of TM polarization. For given values of λ and θ, change of polarization state of the incident wave from TE to TM may lead to a change of the outgoing wave direction, i.e., from deflection ($m = -1$) to specular reflection ($m = 0$). The observed features enable *on–off* switching of ultra-wideband and wide-angle deflection. Both the deflection originated wide band-pass spatial filtering and the specular-reflection originated low-pass spatial filtering, which occur for TE polarization, can be made *on–off* switchable by using *off* state occurring for TM polarization. The same remains true regarding the wide-angle splitting. The above-mentioned properties can also be used for sorting of the TE and TM polarized outgoing waves by redirecting the waves of two different polarizations to two different quadrants, while using $\theta = \theta_1, \theta_2, \ldots, \theta_m$ at λ = const. Moreover, they may enable polarization dependent demultiplexing, for instance, when the incident wave comprises several spectral components. It is noticeable that TM polarization can itself be used to obtain a spatial filtering functionality, i.e., not only as *off* state in the switching scenarios, as observed in the vicinity of λ = 840 nm in Figure 7(a) and (b), and in the vicinity of λ = 560 nm in Figure 5(b). The wide band-pass or the narrow band-pass spatial filtering for $\lambda = \lambda_1$ in TE case and the narrow band-pass spatial filtering for $\lambda = \lambda_2$ in TM case can be obtained in one structure.

3 Conclusions

To summarize, we designed and characterized the ultra-thin meta-array capable in ultra-wideband, wide-angle, single-wave deflection in reflection mode at near-infrared, and examined it for the capability in multifunctional operation enabled by deflection. It is demonstrated that even such a simple structure that is based on Si nanorods working as Mie resonators may yield the highly desirable but unusual deflection features in both the frequency and the incidence-angle domain. Indeed, the designed structure is simpler than the phase-gradient metasurfacs and the blazed gratings, which have more than one element per a large period (supercell). From the wavefront manipulation perspective, ultra-wideband and simultaneously wide-angle deflection connected to the first negative order is probably the most distinguishable result of this study. The deflection region on the wavelength–incidence-angle plane is unusually large and nearly coincides with the region, in which the first negative order is allowed to propagate but higher diffraction orders are not. The –1st order deflection range extends over 1000 nm for wavelength and several tens degrees for incidence angle, while maintaining the efficiency above 80%. The obtained results probably give the first experimental demonstration of ultra-wideband and wide-angle deflection, and the first

demonstration of the diverse deflection regimes and the multifunctionality potential of a simple periodic array based on dielectric resonant nanorods.

Since the aim here was to obtain deflection in a wide but finite, sharply bounded, and frequency dependent range of the incidence angle variation, the possibility of ultimate redistribution of the incident wave energy in favor of the zero order and diffraction orders different from the first negative one is very important. The experimental demonstration of such a redistribution at the smaller-wavelength boundary created by the –2nd order cutoff is especially important because of being required for deflection and band-pass spatial filtering functionalities but is not simply obtainable as compared to the larger-wavelength boundary at the –1st order cutoff. The usefulness of the diffraction orders higher than the –1st one is not restricted in the designed meta-array to the creation of the smaller-wavelength boundary of the –1st order deflection region. In particular, narrow band-pass spatial filtering and splitting with an unusually wide incidence-angle domain response can be enabled by deflection connected with such higher orders. These advanced regimes have not yet been systematically studied, to the best of our knowledge. In addition, some types of spatial filtering, like low-pass and band stop filtering, may occur in the specular-reflection (zero-order) regime. The overall contribution of our study to the spatial filtering research is connected with the demonstration of the different filter types in one structure that is possible when the operating wavelengths are properly chosen. Moreover, the designed structure has a potential in demultiplexing. Thus, various functionalities can be obtained in one relatively simple structure that determines its high potential in wavefront manipulation. Clearly, only one functionality can be used, if necessary.

Change of polarization state of the incident wave can be utilized for switching between deflection and specular-reflection regimes at given wavelength and incidence angle, or within the large deflection region on the wavelength–-incidence-angle plane. In such a manner, spatial filtering and wide-angle splitting can be made *on–off* switchable. Also polarization-yielded *on–off* switching does not need any additional adjustment of the structural parameters. Simplicity of fabrication together with the functional diversity makes the designed structure a perfect candidate for a wavefront manipulating multifunctional device at near-infrared. At the next steps of this research program, we plan to experimentally study the capability of deflection created by the diffraction orders higher than the –1st order, achievable functionalities in the connection with the types of resonances in nanorods, and operation for the circularly polarized waves.

Acknowledgments: A. E. S. thanks Prof. Ph. Lalanne for reading the manuscript, fruitful discussions, and useful suggestions.

Author contribution: All the authors have accepted responsibility for the entire content of this submitted manuscript and approved submission.

Research funding: This work is supported by Narodowe Centrum Nauki (Grant No. 2015/17/B/ST3/00118) and TUBITAK (Fellowship program 2221).

Conflict of interest statement: The authors declare no conflicts of interest regarding this article.

References

[1] C. Ribot, M. S. L. Lee, S. Collin, et al., "Broadband and efficient diffraction," *Adv. Opt. Mater.*, vol. 1, pp. 489–493, 2013.

[2] H. T. Chen, A. J. Taylor, and N. F. Yu, "A review of metasurfaces: physics and applications," *Rep. Prog. Phys.*, vol. 79, p. 076401, 2016.

[3] D. Sell, J. J. Yang, E. W. Wang, T. Phan, S. Doshay, and J. A. Fan, "Ultra-high-efficiency anomalous refraction with dielectric metasurfaces," *ACS Photonics*, vol. 5, pp. 2402–2407, 2018.

[4] M. S. L. Lee, P. Lalanne, J. C. Rodier, and E. Cambril, "Wide-field-angle behavior of blazed-binary gratings in the resonance domain," *Opt. Lett.*, vol. 25, pp. 1690–1692, 2000.

[5] C. Sauvan, P. Lalanne, and M. S. L. Lee, "Broadband blazing with artificial dielectrics," *Opt. Lett.*, vol. 29, pp. 1593–1595, 2004.

[6] K. Hehl, J. Bischoff, U. Mohaupt, et al., "High-efficiency dielectric reflection gratings: design, fabrication, and analysis," *Appl. Opt.*, vol. 38, pp. 6257–6271, 1999.

[7] P. Lalanne, "Waveguiding in blazed-binary diffractive elements," *J. Opt. Soc. Am. A*, vol. 16, pp. 2517–2520, 1999.

[8] M. Oliva, D. Michaelis, F. Fuchs, A. Tunnermann, and U. D. Zeitner, "Highly efficient broadband blazed grating in resonance domain," *Appl. Phys. Lett.*, vol. 102, p. 203114, 2013.

[9] A. E. Serebryannikov, "One-way diffraction effects in photonic crystal gratings made of isotropic materials," *Phys. Rev. B*, vol. 80, p. 155117, 2009.

[10] A. E. Serebryannikov, A. O. Cakmak, and E. Ozbay, "Multichannel optical diode with unidirectional diffraction relevant total transmission," *Opt. Express*, vol. 20, pp. 14980–14990, 2012.

[11] E. Colak, A. E. Serebryannikov, A. O. Cakmak, and E. Ozbay, "Experimental study of broadband unidirectional splitting in photonic crystal gratings with broken structural symmetry," *Appl. Phys. Lett.*, vol. 102, p. 151105, 2013.

[12] P. Rodriguez-Ulibarri, M. Beruete, M. Navarro-Cia, and A. E. Serebryannikov, "Wideband unidirectional transmission with tunable sign-switchable refraction and deflection in nonsymmetric structures," *Phys. Rev. B*, vol. 88, p. 165137, 2013.

[13] P. Li, K. Alam, H. Partanen, M. Kuittinen, G. Kang, and J. Turunen, "Large-angle beaming from asymmetric nanoslit-corrugation structures," *Nanotechnology*, vol. 31, p. 145204, 2020.

[14] N. Yu, P. Genevet, M. A. Kats, et al., "Light propagation with phase discontinuities: generalized laws of reflection and refraction," *Science*, vol. 334, no. 6054, pp. 333–337, 2011.

[15] X. Ni, N. K. Emani, A. V. Kildishev, A. Boltasseva, and V. M. Shalaev, "Broadband light bending with plasmonic nanoantennas," *Science*, vol. 335, no. 6067, p. 427, 2012.

[16] N. Yu and F. Capasso, "Flat optics with designer metasurfaces," *Nat. Mater.*, vol. 13, pp. 139–150, 2014.
[17] F. Ding, A. Pors, and S. I. Bozhevolnyi, "Gradient metasurfaces: a review of fundamentals and applications," *Rep. Prog. Phys.*, vol. 81, p. 026401, 2017.
[18] S. B. Glybovski, S. A. Tretyakov, P. A. Belov, Y. S. Kivshar, and C. R. Simovski, "Metasurfaces: from microwaves to visible," *Phys. Rep.*, vol. 634, pp. 1–72, 2016.
[19] S. M. Kamali, E. Arbabi, A. Arbabi, and A. Faraon, "A review of dielectric optical metasurfaces for wavefront control," *Nanophotonics*, vol. 7, pp. 1041–1068, 2018.
[20] Z. Li, E. Palacios, S. Butun, and K. Aydin, "Visible-frequency metasurfaces for broadband anomalous reflection and high-efficiency spectrum splitting," *Nano Lett.*, vol. 15, pp. 1615–1621, 2015.
[21] B. Yao, X. Zang, Z. Li, et al., "Dual-layered metasurfaces for asymmetric focusing," *Photonics Res.*, vol. 8, pp. 830–843, 2020.
[22] A. Leitis, A. Tittl, M. Liu, et al., "Angle-multiplexed all-dielectric metasurfaces for broadband molecular fingerprint retrieval," *Sci. Adv.*, vol. 5, p. eaaw2871, 2019.
[23] Y. F. Yu, A. Y. Zhu, R. Paniagua-Dominguez, Y. H. Fu, B. Luk'yanchuk, and A. I. Kuznetsov, "High-transmission metasurface with 2π phase control at visible frequencies," *Laser Photonics Rev.*, vol. 9, pp. 412–418, 2015.
[24] M. Liu, O. L. Yang, A. A. Rifat, et al., "Deeply subwavelength metasurface resonators for terahertz wavefront manipulation," *Adv. Opt. Mater.*, vol. 7, p. 1900736, 2019.
[25] T. Matsui, A. Miura, N. Ikeda, et al., "Experimental investigation of double-groove grating satisfying total internal reflection condition," *Opt. Express*, vol. 22, pp. 25362–25370, 2014.
[26] A. Ozer, N. Yilmaz, H. Kocer, and H. Kurt, "Polarization-insensitive beam splitters using all-dielectric phase gradient metasurfaces at visible wavelengths," *Opt. Lett.*, vol. 43, pp. 4350–4353, 2018.
[27] M. Khorasaninejad, A. Ambrosio, P. Kanhaiya, and F. Capasso, "Broadband and chiral binary dielectric meta-holograms," *Sci. Adv.*, vol. 2, p. e1501258, 2016.
[28] A. E. Serebryannikov, P. Lalanne, A. Y. Petrov, and E. Ozbay, "Wide-angle reflection-mode spatial filtering and splitting with photonic crystal gratings and single-layer rod gratings," *Opt. Lett.*, vol. 39, pp. 6193–6196, 2014.
[29] A. E. Serebryannikov, A. Lakhtakia, M. Aalizadeh, E. Ozbay, and G. A. E. Vandenbosch, "Temperature-mediated invocation of the vacuum state for switchable ultrawide-angle and broadband deflection," *Sci. Rep.*, vol. 8, p. 15044, 2018.
[30] Z.-L. Deng, S. Zhang, and G. Ping Wang, "A facile grating approach towards broadband, wide-angle and high-efficiency holographic metasurfaces," *Nanoscale*, vol. 8, pp. 1588–1594, 2016.
[31] M. Lester and D. C. Skigin, "Coupling of evanescent *s*-polarized waves to the far field by waveguide modes in metallic arrays," *J. Opt. A Pure Appl. Opt.*, vol. 9, pp. 81–87, 2007.
[32] Y. Han, Q. Li, S. Zhu, K. W. Ng, and K. M. Lau, "Continuous-wave lasing from InP/InGaAs nanoridges at telecommunication wavelengths," *Appl. Phys. Lett.*, vol. 111, p. 212101, 2017.
[33] A. Baron, E. Devaux, J.-C. Rodier, et al., "Compact antenna for efficient and unidirectional launching and decoupling of surface plasmons," *Nano Lett.*, vol. 11, pp. 4207–4212, 2011.
[34] H. F. Ma, X. Shen, Q. Cheng, W. X. Jiang, and T. J. Cui, "Broadband and high-efficiency conversion from guided waves to spoof surface plasmon polaritons," *Laser Photonics Rev.*, vol. 8, pp. 146–151, 2014.
[35] W. Wang, S. Wu, K. Reinhardt, Y. Lu, and S. Chen, "Broadband light absorption enhancement in thin-film silicon solar cells," *Nano Lett.*, vol. 10, pp. 2012–2018, 2010.
[36] G. Quaranta, G. Basset, O. J. F. Martin, and B. Gallinet, "Recent advances in resonant waveguide gratings," *Laser Photonics Rev.*, vol. 12, p. 1800017, 2018.
[37] M. Memarian, X. Li, Y. Morimoto, and T. Itoh, "Wide-band/angle blazed surfaces using multiple coupled blazing resonances," *Sci. Rep.*, vol. 7, p. 42286, 2017.
[38] F. Ding, Y. Chen, and S. Bozhevolnyi, "Gap-surface plasmon metasurfaces for linear-polarization conversion, focusing, and beam splitting," *Photonics Res.*, vol. 8, pp. 707–714, 2020.
[39] Y. Zhang, L. Shi, D. Hu, et al., "Full-visible multifunctional aluminium metasurfaces by in situ anisotropic thermoplasmonic laser printing," *Nanoscale Horiz.*, vol. 4, pp. 601–609, 2019.
[40] K. Chen, G. Ding, G. Hu, et al., "Directional janus metasurface," *Adv. Mater.*, vol. 32, p. 1906352, 2020.
[41] A. E. Serebryannikov, K. B. Alici, T. Magath, A. O. Cakmak, and E. Ozbay, "Asymmetric Fabry-Perot-type transmission in photonic-crystal gratings with one-sided corrugations at a two-way coupling," *Phys. Rev. A*, vol. 86, p. 053835, 2012.
[42] D. Sell, J. Yang, R. Yang, and J. A. Fan, "Large-angle, multifunctional metagratings based on freeform multimode geometries," *Nano Lett.*, vol. 17, pp. 3252–3257, 2017.
[43] D. Sell, J. Yang, S. Doshay, and J. A. Fan, "Periodic dielectric metasurfaces with high-efficiency, multiwavelength functionalities," *Adv. Opt. Mater.*, vol. 5, p. 1700645, 2017.
[44] X. Wang, J. Ding, B. Zheng, S. An, G. Zhai, and H. Zhang, "Simultaneous realization of anomalous reflection and transmission at two frequencies using bi-functional metasurfaces," *Sci. Rep.*, vol. 8, p. 1876, 2018.
[45] V. Vashistha, M. Krawczyk, A. E. Serebryannikov, and G. A. E. Vandenbosch, "Light guiding, bending, and splitting via local modification of interfaces of a photonic waveguide," *Opt. Lett.*, vol. 44, pp. 4725–4728, 2019.
[46] T. Cai, S. Tang, G. Wang, et al., "High performance bifunctional metasurfaces in transmission and reflection geometries," *Adv. Opt. Mater.*, vol. 5, p. 1600506, 2017.
[47] T. Cai, G.-M. Wang, H.-X. Xu, S.-W. Tang, H. Li, and J.-G. Liang, "Bifunctional Pancharatnam–Berry metasurface with high-efficiency helicity-dependent transmissions and reflections," *Ann. Phys. (Berlin)*, vol. 530, p. 1700321, 2017.
[48] J. P. B. Mueller, N. A. Rubin, R. C. Devlin, B. Groever, and F. Capasso, "Metasurface polarization optics: independent phase control of arbitrary orthogonal states of polarization," *Phys. Rev. Lett.*, vol. 118, p. 113901, 2017.
[49] D. Wen, F. Yue, G. Li, et al., "Helicity multiplexed broadband metasurface holograms," *Nat. Commun.*, vol. 6, p. 8241, 2015.
[50] Z.-L. Deng, Y. Cao, X. Li, and G. P. Wang, "Multifunctional metasurface: from extraordinary optical transmission to extraordinary optical diffraction in a single structure," *Photonics Res.*, vol. 6, pp. 443–450, 2018.
[51] J. R. Cheng, S. Inampudi, and H. Mosallaei, "Optimization-based dielectric metasurfaces for angle-selective multifunctional beam deflection," *Sci. Rep.*, vol. 7, p. 12228, 2017.

[52] M. Veysi, C. Guclu, O. Boyraz, and F. Capolino, "Thin anisotropic metasurfaces for simultaneous light focusing and polarization manipulation," *J. Opt. Soc. Am. B*, vol. 32, pp. 318–323, 2015.
[53] S. Boroviks, R. A. Deshpande, N. A. Mortensen, and S. I. Bozhevolnyi, "Multifunctional metamirror: polarization splitting and focusing," *ACS Photonics*, vol. 5, pp. 1648–1653, 2018.
[54] N. Mahmood, I. Kim, M. Q. Mehmood, et al., "Polarisation insensitive multifunctional metasurfaces based on all-dielectric nanowaveguides," *Nanoscale*, vol. 10, pp. 18323–18330, 2018.
[55] E. Maguid, I. Yulevich, M. Yannai, V. Kleiner, M. L. Brongersma, and E. Hasman, "Multifunctional interleaved geometric-phase dielectric metasurfaces," *Light Sci. Appl.*, vol. 6, p. e17027, 2017.
[56] G. Ding, K. Chen, X. Luo, J. Zhao, T. Jiang, and Y. Feng, "Dual-helicity decoupled coding metasurface for independent spin-to-orbital angular momentum conversion," *Phys. Rev. Appl.*, vol. 11, p. 044043, 2019.
[57] Q. Wang, E. T. F. Rogers, B. Gholipour, et al., "Optically reconfigurable metasurfaces and photonic devices based on phase change materials," *Nat. Photonics*, vol. 10, pp. 60–65, 2016.
[58] K. Dong, S. Hong, Y. Deng, et al., "A lithography-free and field-programmable photonic metacanvas," *Adv. Mater.*, vol. 30, p. 1703878, 2018.
[59] Q. He, S. Sun, and L. Zhou, "Tunable/reconfigurable metasurfaces: physics and applications," *Research*, vol. 2019, p. 1849272, 2019.
[60] Y. Li, J. Lin, H. Guo, W. Sun, S. Xiao, and L. Zhou, "A tunable metasurface with switchable functionalities: from perfect transparency to perfect absorption," *Adv. Opt. Mater.*, vol. 8, p. 1901548, 2020.
[61] L. Maigyte and K. Staliunas, "Spatial filtering with photonic crystals," *Appl. Phys. Rev.*, vol. 2, p. 011102, 2015.
[62] D. R. Abujetas, R. Paniagua-Domínguez, and J. A. Sánchez-Gil, "Unraveling the Janus role of Mie resonances and leaky/guided modes in semiconductor nanowire absorption for enhanced light harvesting," *ACS Photonics*, vol. 2, pp. 921–929, 2015.
[63] R. Petit, Ed., *Electromagnetic Theory of Gratings*, Berlin Heidelberg:Springer, 1980.
[64] D. Headland, E. Carrasco, S. Nirantar et al., "Dielectric resonator reflectarray as high-efficiency nonuniform terahertz metasurface," *ACS Photonics*, vol. 3, pp. 1019–1026, 2016.
[65] L. Dettwiller and P. Chavel, "Optical spatial filtering using interferences," *J. Opt. Soc. Am. A*, vol. 1, pp. 18–27, 1984.
[66] D. Schurig and D. R. Smith, "Spatial filtering using media with indefinite permittivity and permeability tensors," *Appl. Phys. Lett.*, vol. 82, pp. 2215–2217, 2003.
[67] C. Rizza, A. Ciattoni, E. Spinozzi, and L. Columbo, "Terahertz active spatial filtering through optically tunable hyperbolic metamaterials," *Opt. Lett.*, vol. 37, pp. 3345–3347, 2012.
[68] L. V. Alekseyev, E. E. Narimanov, T. Tumkur, et al., "Uniaxial epsilon-near-zero metamaterial for angular filtering and polarization control," *Appl. Phys. Lett.*, vol. 97, p. 131107, 2010.
[69] R. Rabady and I. Avrutsky, "Experimental characterization of simultaneous spatial and spectral filtering by an optical resonant filter," *Opt. Lett.*, vol. 29, pp. 605–607, 2004.
[70] W.-N. Liu, R. Chen, W.-Y. Shi, K.-B. Zeng, F.-L. Zhao, and J.-W. Dong, "Narrow-frequency sharp-angular filters using all-dielectric cascaded meta-gratings," *Nanophotonics*, vol. 9, p. 20200141, 2020.
[71] A. E. Serebryannikov, A. Y. Petrov, and E. Ozbay, "Toward photonic crystal based spatial filters with wide angle ranges of total transmission," *Appl. Phys. Lett.*, vol. 94, p. 181101, 2009.
[72] S. Gawali, D. Gailevicius, G. Gerre-Werner, et al., "Photonic crystal spatial filtering in broad aperture diode laser," *Appl. Phys. Lett.*, vol. 115, p. 141104, 2019.
[73] V. Purlys, L. Maigyte, D. Gailevicius, M. Peckus, M. Malinauskas, and K. Staliunas, "Spatial filtering by chirped photonic crystals," *Phys. Rev. A*, vol. 87, p. 033805, 2013.
[74] P. Lalanne, J. Hazart, P. Chavel, E. Cambril, and H. Launois, "A transmission polarizing beam splitter grating," *J. Opt. A Pure Appl. Opt.*, vol. 1, pp. 215–219, 1999.
[75] B. A. Slovick, Y. Zhou, Z. G. Yu, et al., "Metasurface polarization splitter," *Philos. Trans. R. Soc. A*, vol. 375, p. 20160072, 2017.
[76] M. Khorasaninejad, W. Zhu, and K. B. Crozier, "Efficient polarization beam splitter pixels based on a dielectric metasurface," *Optica*, vol. 2, pp. 376–382, 2015.

Supplementary Material: The online version of this article offers supplementary material (https://doi.org/10.1515/nanoph-2020-0386).